Numerical investigations on the rubbing process in labyrinth seals for full flight mission

Oliver Munz, Lisa Hühn, Fabian Bleier and Hans-Jörg Bauer
oliver.munz@kit.edu
Institute of Thermal Turbomachinery
Karlsruhe Institute of Technology
76131 Karlsruhe
Germany

ABSTRACT

Labyrinth seals are a commonly used sealing technology to prevent and control leakage flows at rotor-stator interfaces in turbo machinery. Small clearances required by higher pressure ratios and the economical use of cooling air lead to potential rubbing events. These may cause detrimental heat input into the rotating structure and can lead to severe damages. Honeycomb liners on the stator part tolerate rubbing events to a certain extent and therefore allow for smaller gap widths, which lead to minimal leakage.

A unique and independently developed one-dimensional numerical model is used to investigate critical rubbing conditions in a typical aircraft flight mission. It considers kinematic contact conditions, friction, heat conduction and abrasive and plastic wear. This model allows the calculation of the loads, such as the contact pressures and temperatures on the components. First experimental investigations for an idealized contact between a metal foil, representing the honeycomb part, and a rotating seal fin are used to validate the model. Then, predictions of engine performance calculations are additionally used to calculate input parameters for the one-dimensional model. These are the relative contact velocity and the casing temperature of the honeycomb.

Finally, the results of the one-dimensional rubbing model such as rub forces, temperatures and wear of the seal fin or the honeycomb liner are compared for five different operating points of the flight mission: Ground idle, Takeoff, Cruise, Approach, Re-slam. Based on these results, damaging effects on the sealing system are evaluated and the most critical operating point, in this case the Re-slam, could be identified.

Keywords: labyrinth seal; rubbing process; honeycomb; engine performance; aircraft flight mission; load prediction

NOMENCLATURE

Latin

E	Young's modulus	[N/m^2]
h	heat transfer coefficient	[W/m^2 K]
k	stiffness coefficient	[N/m^3]
p	pressure	[MPa]
r	radius	[mm]
R	yield strength	[N/m^2]
$\dot{q}$	heat flux	[W/m^2]
s	incursion	[mm]
T	temperature	[K]
v	velocity	[m/s]
w	wear	[m]

Greek

β	heat partitioning factor	[-]
μ	coefficient of friction	[-]

Subscripts

φ	circumference
a	abrasive
ax	axial
C	nominal contact
$foil$	metal foil
$fric$	friction
i	initial
pl	plastic
rad	radial
sf	seal fin
tot	total

1.0 INTRODUCTION

In order to reduce or control leakage mass flows between static and rotating components, labyrinth seals are state of the art in gas and steam turbines [1]. The main parameters for the leakage mass flow through a labyrinth seal are the gap width between sealing tip and stator and the pressure ratio across the seal [2,3]. High pressure ratios and high combustion temperatures, as they occur in modern gas turbines and especially in aircraft engines, require efficient use of cooling air and high component efficiencies. By reducing the sealing gap width, the efficiency of the gas turbine can be increased, and fuel consumption reduced. However, a small gap can lead to contact between the rotor and stator during rapid changes in operation and manoeuvre loads. In such a so-called rubbing process, the sudden release of frictional heat may cause a harmful temperature rise and thus critical damage to the rotor [4]. Therefore, abradable liners are used which guarantee targeted and rapid wear of the stator and thus protect the rotor from damage.

Some experimental investigations were carried out on the rubbing process between labyrinth seals and honeycombs with the focus on different coating materials and temperature resistances [5–11]. However, there is a lack of experimental and numerical investigations, which enable the investigation of the fundamental physical mechanisms. Pychynski et al. [12] introduced the experimental setup depicted in Figure 1. The complex honeycomb structure is idealized to the contact between a single metal foil representing the double wall section and a seal fin. The test rig allows to determine the influence of the rubbing parameters relative velocity, incursion rate and incursion depth on resulting contact forces, temperatures and wear for stainless steel material combinations. On the basis of the experimental investigation Pychynski [13] further developed a modelling approach. Munz et al. [14] performed a sensitivity analysis for the nickel-based alloys most commonly used in turbines. Fischer et al. [15] used the

experimental data to validate a finite element model of the rubbing contact taking into account an advanced friction law, von Mises plasticity and a ductile failure criterion.

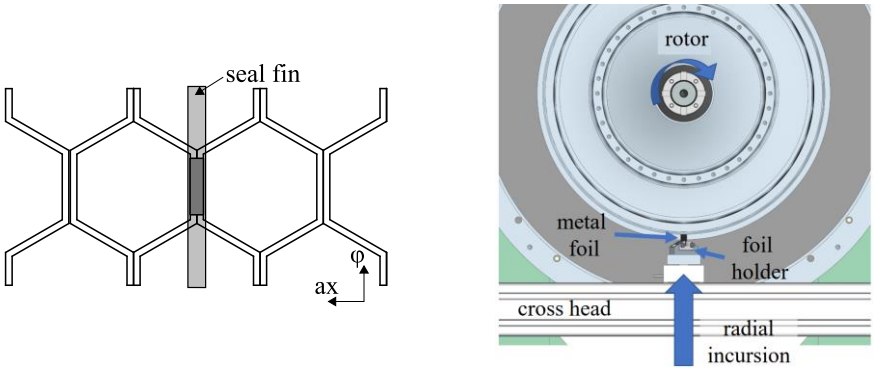

Figure 1 Idealized contact on the honeycomb double wall section and experimental setup, modified from [16]

In this study, the model of the rubbing process introduced by Pychynski [13] is used to calculate contact temperatures, contact pressures and wear for different operating points in a flight mission of an aircraft. The method used is illustrated in Figure 2. The input parameters for the flight mission calculations are taken from a typical flight cycle of a regional commercial jet. The calculation of the relevant quantities is explained in more detail in section 2.0. Furthermore, the model of Pychynski [13] is calibrated with experimental data from the test bench shown in Figure 1 (section 3.0 and 4.0). With this set of model result data, the load on the seal fin is evaluated and the most critical operating points are identified.

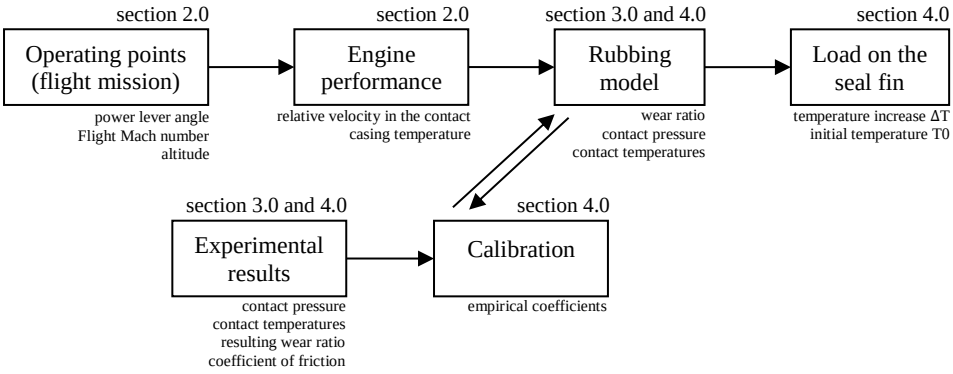

Figure 2 Flow diagram of the investigation with the individual modules of the simulation, the computed quantities and the corresponding section.

2.0 ENGINE PERFORMANCE

For the estimation of boundary values for the model a gas turbine performance software (GasTurb [17]) is used. The software offers an existing model of a twin-shaft geared turbofan with a design bypass ratio of 12. The fan has a diameter of 2.36 m and is driven by a transmission gear with a ratio of 2.5. The coupled low-pressure compressor consists of three stages, the high-pressure compressor has nine stages. The high-pressure turbine consists of two stages and the low-pressure turbine has three stages. These values are in the range for the variants of the PW1000G by Pratt & Whitney. The aim of the study is to indicate a trend and not to claim to be a quantitative calculation for a specific engine.

2.1 Flight mission

The data consists of a steady state off-design calculation of a typical flight mission and a transient simulation of a “hot Re-slam” at the end of the mission. The flight mission depicted in Figure 3 is extracted from [18] and compared to a flight profile recorded onboard a regional commercial jet [19]. For this study, four operating points are

considered: Ground Idle, Takeoff, Cruise and Approach. The resulting altitude, Mach number and power setting are depicted in Figure 3 and used as an input for GasTurb. The power lever angle (PLA) setting was adjusted according to the rotational speed of the high-pressure shaft. All calculations were carried out at International Standard Atmosphere (ISA).

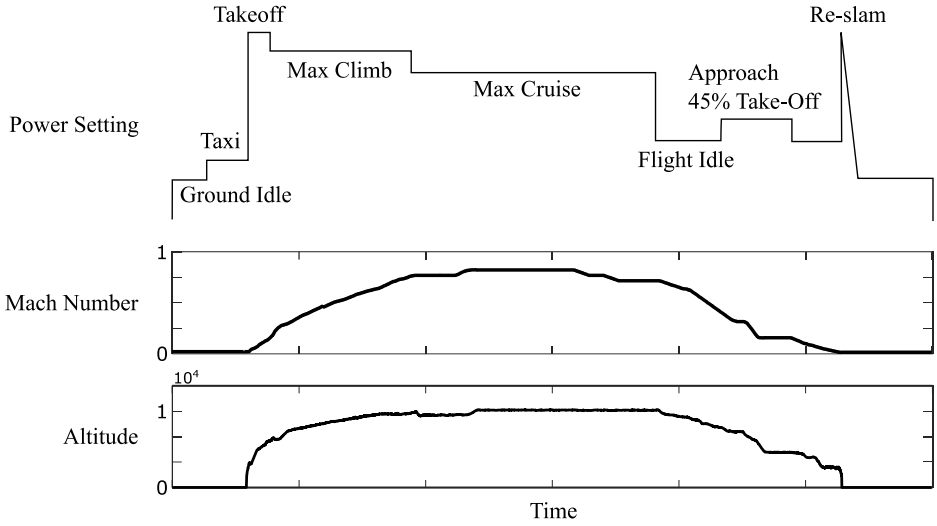

Figure 3 Typical flight cycle, modified from [18] and [19]

At the end of the flight mission a "Re-slam" was simulated. The "Re-slam" is a flight manoeuvre in which the aircraft is in the landing approach but must perform an emergency takeoff. Because the casing temperatures in the engine are very low during the landing approach and the rotor disks are still relatively hot, a sudden acceleration leads to a minimal gap clearance. Therefore, it is an operating point of the engine at which it is most likely that rubbing processes take place [20].

2.2 Operating points

The calculated engine parameters for each operating point are depicted in Table 1. The labyrinth seal fin considered in this study is located at the shroud of the first high-pressure turbine disk. The radius of the blade tip is about 278 mm. With the speed of the high-pressure spool, the relative velocity is calculated. The software was also used to estimate the casing temperature of the first turbine stage. This was determined by using a design point calculation with the burner exit temperature T4 and flight altitude for the different operating points. These boundary conditions are applied in the rubbing model to calculate the load on the seal fin.

Table 1 Data for flight mission

Description	Unit	Ground Idle	Takeoff	Cruise	Approach	Re-slam
Altitude	m	180	180	10668	1800	500
Mach Number	-	0	0	0,8	0,5	0,3
PLA	%	25	80	75	40	80
Net Thrust	kN	15,8	118,0	29,9	5,1	123,4
HP Spool Speed	rpm	8593	14347	13824	10162	15376
LP Spool Speed	rpm	3166	6570	7454	4432	7760
Burner Exit Temperature (T4)	K	1158	1674	1549	1251	1814
Casing Temperature	K	760	950	780	765	1003
Relative velocity	m/s	250	418	403	296	448

3.0 RUBBING MODEL

The rubbing model represents the experimental setup as described in Figure 1 and the applied boundary conditions are depicted in Figure 4. It follows a one-dimensional approach and all parameters describe macroscopic quantities. The rotor has a diameter of 360 mm. The seal fin is 4 mm high and has a width of 0.6 mm. The stationary metal foil has the dimensions 20x12 mm with a variable thickness from 0.3 to 0.6 mm.

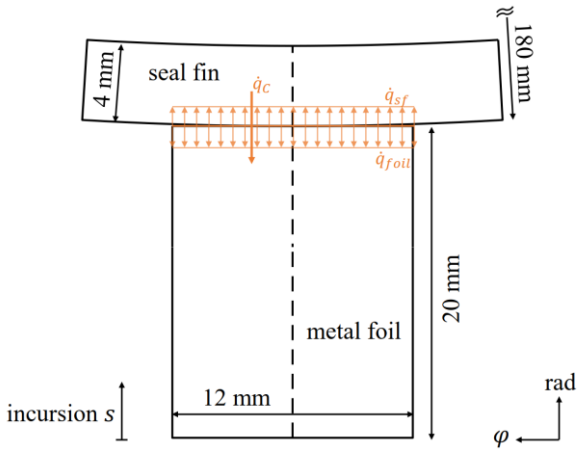

Figure 4 Boundary conditions of the rubbing model

It is assumed that the metal foil and the seal fin are in continuous contact and the contact pressure p_C is distributed uniformly over the nominal contact area. Therefore, the contact pressure p_C is a function of the incursion s:

$$p_C = s\,k. \tag{1}$$

The pressure-dependent radial stiffness k is calculated for the geometry of the metal foil, seal fin and foil holder of the test rig. The calculation of the incursion s takes into account the constant incursion of the foil base, thermal expansion of the metal foil and wear. Coulomb's law of friction is used with a constant and uniform coefficient of friction and must be obtained from experimental results. Therefore, the friction heat flux

$$\dot{q}_{fric} = \mu\, p_C\, v_\varphi \tag{2}$$

is only a function of relative velocity and contact pressure. For determining the contact pressure, friction and wear behaviour the prediction of the resulting temperatures is crucial. For this, a thermal contact model is implemented.

3.1 Thermal contact model

The dissipation of the friction energy is a process that takes place on a microscopic scale. An initial heat partitioning factor β_i is introduced in order to determine the resulting macroscopic heat fluxes:

$$\dot{q}_{foil} = \beta_i\, \dot{q}_{fric}, \tag{3}$$

$$\dot{q}_{sf} = (1-\beta_i)\, \dot{q}_{fric}. \tag{4}$$

Thus, and with the assumption of an initial even heat partitioning ($\beta_i = 0.5$), the heat flux into the seal fin $\dot{q}_{sf}$ and into the metal foil $\dot{q}_{foil}$ can be calculated. The contact is assumed to be perfect. Due to the different materials and temperatures, a heat flux

$$\dot{q}_C = h_C \left(T_{C,foil} - T_{C,sf}\right) \tag{5}$$

is consequently formed from the seal fin to the metal foil with the heat transfer coefficient h_C. The heat transport from the seal fin to the foil interacts with the initial heat partitioning so that the effective heat partitioning β_{eff} can be determined. It is a function of the temperatures of seal fin and metal foil, the area of the contact, the initial

heat partitioning factor, and the heat transfer coefficient. The resulting heat fluxes from the thermal contact model are applied as input parameters to numerical finite difference models for the seal fin and metal foil. Convective cooling, radiation and the effect of moving heat source because of the relative velocity are also considered.

3.2 Wear model

The total wear of the metal foil is composed of the abrasive wear w_a and the plastic wear w_{pl}:

$$w_{tot} = w_a + w_{pl}. \tag{6}$$

The abrasive wear is modelled by Archard's law of wear and a viscoplastic wear model is used. The corresponding equations are attached to the Appendix. The percentage of dominant wear conditions can be described using the wear ratio w_a/w_{tot}. A wear ratio greater than 0.5 is therefore indicating a higher amount of abrasive wear. The empirical equations used for abrasive and plastic wear as well as the heat transfer coefficient must be determined based on experimental data.

No significant wear of the seal fin was observed during the experimental investigation. Therefore, it is neglected in the model.

3.3 Material properties and calibration

The material properties for the rotor material Inconel 718 and the foil material Hastelloy X were taken from data sheets by the manufacturers Haynes International [21] and Special Metals [22]. They are implemented as a function of the one-dimensional temperature distribution. An extract of the material parameters used is given in Table 2 for ambient temperature and 1000°C.

Table 2 Selection of the material properties for Inconel 718 and Hastelloy X at two arbitrary temperatures (Young's modulus E, yield strength at 0.2% offset R_{p02}, thermal conductivity λ, specific heat c_p, coefficient of thermal expansion α)

Inconel 718	E in GPa	R_{p02} in MPa	λ in $\frac{W}{m\,K}$	c_p in $\frac{J}{kg\,K}$	α in $10^{-6}\,\frac{1}{K}$
20 °C	204	1030	11,52	460	14,1
1000 °C	134	640	25,80	637	17,4
Hastelloy X					
20 °C	205	378	9,18	486	13,0
1000 °C	141	83	27,20	809	15,6

The parameters for the abrasive and plastic wear model and the heat transfer coefficient in the contact were adjusted so that the resulting contact pressure, the resulting foil temperature near the contact $T_{C,foil}$ and the wear ratio are consistent with the experimental reference scenario. The calibrated model parameter are summed up in Table 3. In addition, the coefficient of friction determined from the experiment is given.

Table 3 Calibrated model parameters

$h_{C,0}$	proportionality factor of contact heat transfer	[1/m]	20616
$k_{w,a}$	abrasive wear coefficient	[-]	19,25
t_{pl}	time constant for plastic wear	[ms]	39,8
μ	coefficient of friction	[-]	0,09

For further information regarding the model and validation please refer to Pychynski [13] and Munz et al. [14]. To calculate the resulting contact pressures, friction temperatures and wear rates, with the model described here, input parameters in the form of relative velocity and ambient temperature are necessary.

4.0 RESULTS

In order to investigate the five critical flight conditions with the model, the behaviour of the results for increasing relative velocity and casing temperatures is first discussed. The model described in section 3.0 was calibrated with experimental results from the rubbing test rig. For calibration and validation, a scenario with a relative velocity of 110 m/s, the incursion rate 0.25 mm/s and a final incursion depth of 1 mm was used.

4.1 Increasing relative velocity

Figure 5 depicts the simulated foil temperature at the contact, contact pressure and the resulting wear ratio as a function of the relative velocity. The contact pressure and foil temperature are averaged over the duration of the rubbing process. The wear ratio is the final result of the process, which is determined after the experimental test by weight loss. The experimental reference point used for calibration is also illustrated.

The first observation is that the development of the temperature near the contact $T_{C,foil}$ in Figure 5 a) shows a significant increase up to approx. 200 m/s. Then the gradient decreases and a nearly stationary section develops. This behaviour is consistent with experimental results [12] and the numerical investigation of Fischer et al. [15]. The contact pressure depicted in Figure 5 b) is decreasing with increasing relative velocity. As the relative velocity increases, more frictional heat is released in the contact surface (see eq. (2)) and therefore the temperature of the metal foil increases. Thereby the Young's modulus of elasticity and the yield strength of the material are reduced which leads to decreasing contact pressures. The wear ratio shown in Figure 5 c) exhibits only a very low sensitivity to the increasing relative velocity and has approx. a value of a 0.2 throughout the whole range of relative velocities. Consequently, mainly plastic wear is present.

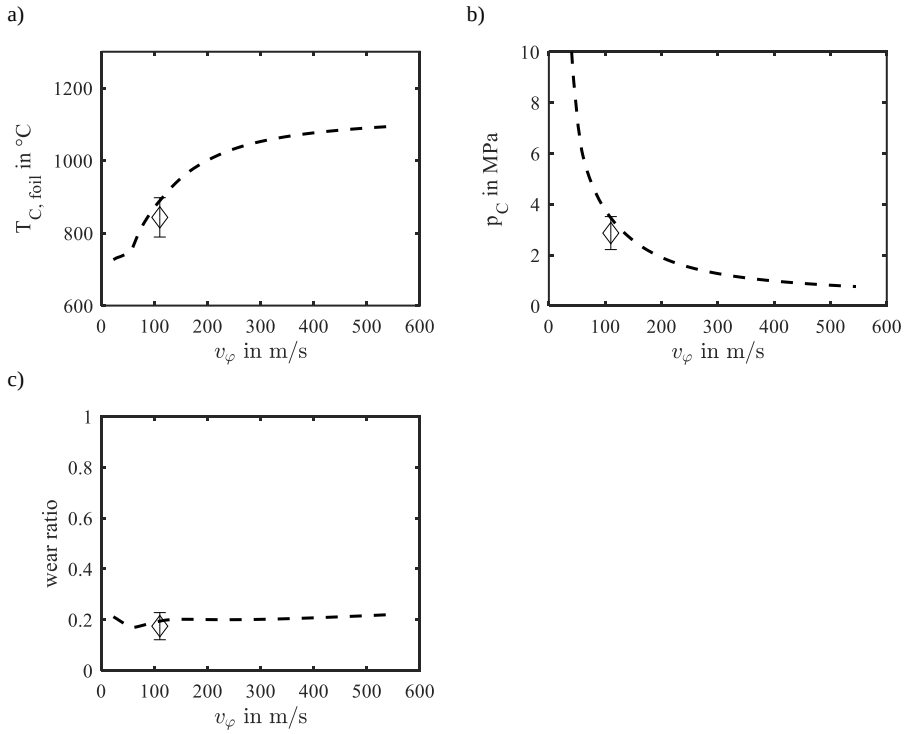

Figure 5 Predicted foil temperature in the contact, contact pressure and resulting wear ratio as a function of the relative velocity v_φ in the contact and the experimental reference point

4.2 Increasing casing temperature

Figure 6 depicts the simulated foil temperature at the contact, contact pressure and the resulting wear ratio as a function of the casing temperature. The experimental investigation is carried out in ambient conditions. In order to simulate changing boundary conditions of the engine, the ambient temperature and the initial temperature

of the metal foil as well as the seal fin were initialized with the temperature of the casing.

The foil temperature depicted in Figure 6 a) increases with increasing casing temperature. The friction power released in the contact continues to cause the system to heat up. As the casing temperature in Figure 6 b) increases, the contact pressure decreases as described in section 4.1. With increasing casing temperatures, the wear ratio also decreases (see Figure 6 c). The increasing temperature leads to an earlier activation of plastic wear and thus to an even lower proportion of abrasive wear. Both, the relative velocity as well as the casing temperature have similar effects on the resulting contact pressures, contact temperatures and wear ratios. In the flight cycle operating points both factors change simultaneously.

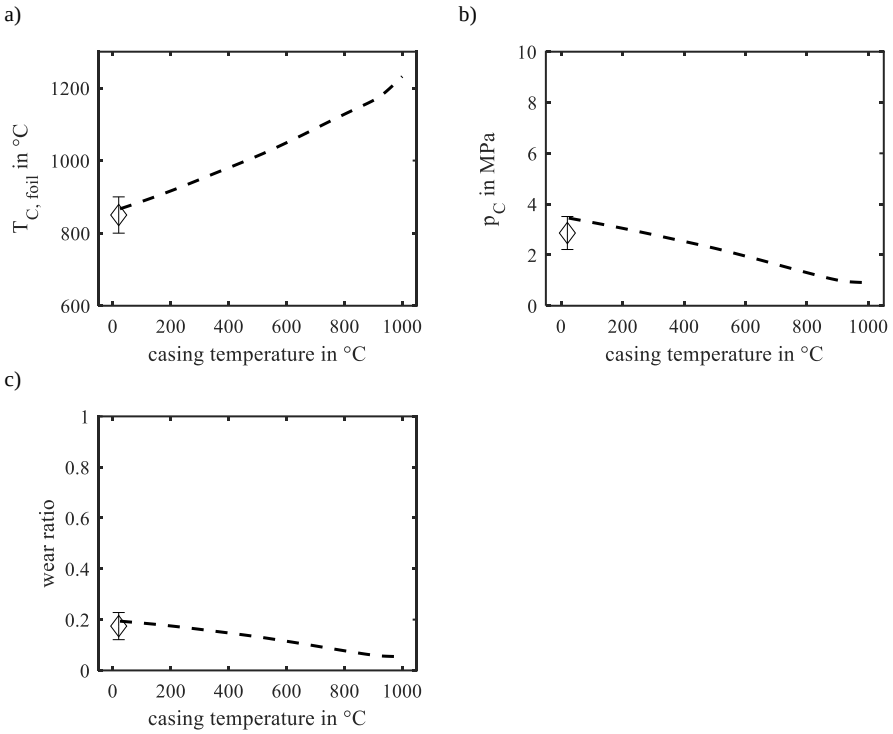

Figure 6 Predicted foil temperature in the contact, contact pressure and the resulting wear ratio as a function of the casing temperature and the experimental reference point

4.3 Operating points

As a next step, the resulting relative velocities and casing temperatures from the flight mission calculation in Table 1 are used as input for the rubbing model. The predicted contact pressure is shown in Figure 7. The contact pressure does not vary significantly and is relatively low due to the increased initial temperature of metal foil and seal fin. Therefore, the main part of the load on the seal fin is due to thermal expansion in the contact region.

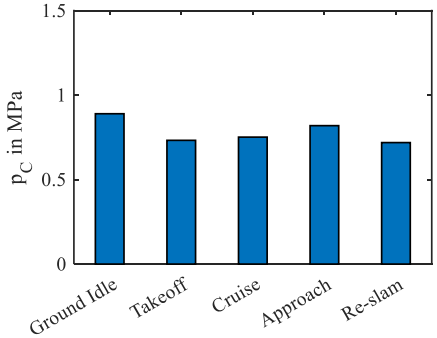

Figure 7 Predicted contact pressure as a function of the flight cycle operating points

The temperatures of the seal fin and the metal foil near the contact are depicted in Figure 8. Additionally the initial temperature T0 (■) and the temperature increase due to the rubbing process ΔT (■) is indicated. It can clearly be seen that the temperature increase of the metal foil (Figure 8 a) is much more pronounced then the temperature increase of the seal fin (Figure 8 b). This can be explained by the effect of the moving heat source. While the contact of the metal foil always takes place at a stationary point, the contact spot on the seal fin moves out of the contact. Only after almost a complete revolution does this point meet the hot metal foil again. During this time, it is cooled by the surrounding air. It is therefore much cooler than the metal foil. According to Pychynski [4], this local temperature increase of the seal fin represents one of the most important parameters with respect to the stress of the seal fin.

For Ground Idle, Cruise and Approach the initial temperature of the metal foil are quite similar, but the temperature increase is more pronounced for the Cruise operating point. This can be attributed to the higher relative velocity. The highest contact temperatures both for the metal foil and the seal fin occur for Takeoff and Re-slam. This corresponds to the operating conditions with the highest initial temperatures and the highest relative velocities. In Hühn et al. [23] it could be shown that with a rotor initial temperature $T0$ of 500 °C and a temperature increase of delta ΔT = 400 °C, the temperature-dependent tensile strength decreases by almost 57 %.

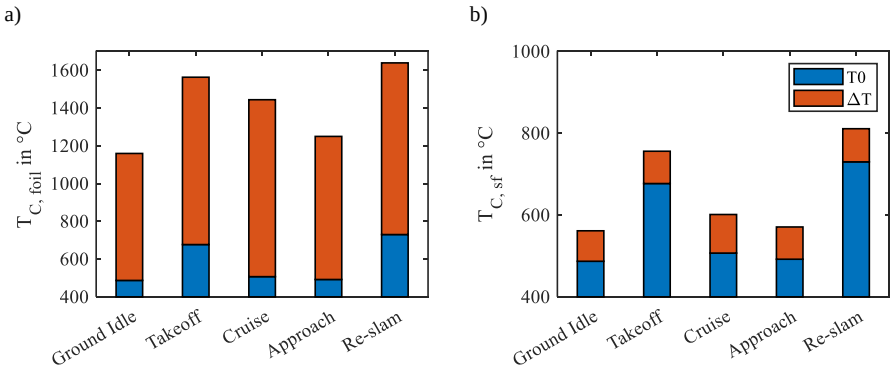

Figure 8 Predicted temperature of the foil and seal fin at the contact as a function of the flight cycle operating points

5.0 CONCLUSIONS

In this paper, a typical flight mission of a regional commercial jet was used to derive boundary conditions for an independently developed model of the rubbing process. With the help of a gas turbine performance software, process parameters for an engine were calculated from the altitude and speed of the aircraft and the position of the thrust lever. For a labyrinth seal situated on the shroud of the first turbine stage, the relative speed and casing temperature could be calculated. The results for the operating points Ground Idle, Takeoff, Cruise, Approach and Re-slam were used in the rubbing model to identify the thermal load on the seal fin.

With the obtained results, it was shown that an increase in relative velocity and casing temperature leads to decreasing contact pressures and increasing temperatures due to friction energy released in the contact. The thermal load resulting from the local temperature increase in the contact area of the seal fin was highest for the Re-slam condition. Using the method presented for a generic engine, the load on the seal fin as a result of a rubbing incident could be determined. With the help of more complex and realistic boundary conditions, it will be possible to optimize the sealing system with regard to the rubbing behaviour for a specific engine.

The further experimental investigation of the rubbing process for several operating points is planned and urgently necessary. An adaptation of the model using these data and a more detailed investigation of heat partitioning is an important measure to

understand the rubbing process more deeply. This ultimately makes it possible to derive appropriate actions to increase the safety and efficiency of the sealing system.

ACKNOWLEDGEMENTS

This work is a result of the research project BA 2848/5-1. We are grateful for funding by the DFG (Deutsche Forschungsgemeinschaft).

REFERENCES

[1] R. E. Chupp, R. C. Hendricks, S. B. Lattime, and B. M. Steinetz, "Sealing in Turbomachinery," *Journal of Propulsion and Power*, vol. 22, no. 2, pp. 313–349, 2006.

[2] E. Braun, K. Dullenkopf, and H.-J. Bauer, "Optimization of Labyrinth Seal Performance Combining Experimental, Numerical and Data Mining Methods," in *ASME Turbo Expo 2012: Turbine Technical Conference and Exposition*, p. 1847, 2012.

[3] V. Schramm, K. Willenborg, S. Kim, and S. Wittig, "Influence of a Honeycomb Facing on the Flow Through a Stepped Labyrinth Seal," in *ASME Turbo Expo 2000: Power for Land, Sea, and Air*, V003T01A092, May 8-11, 2000.

[4] T. Pychynski, K. Dullenkopf, and H.-J. Bauer, "Theoretical Study on the Origin of Radial Cracks in Labyrinth Seal Fins due to Rubbing," in *ASME Turbo Expo 2013: Turbine Technical Conference and Exposition*, pp. V07AT27A006, 2013.

[5] R. C. Bill and L. P. Ludwig, "Wear of seal materials used in aircraft propulsion systems," *Wear*, vol. 59, no. 1, pp. 165–189, 1980.

[6] R. C. Bill and L. T. Shiembob, "Friction and Wear of Sintered Fibermetal Abradable Seal Materials," *Journal of Lubrication Technology*, vol. 99, no. 4, p. 421, 1977.

[7] P. Dowson, S. L. Ross, and C. Schuster, "The investigation of suitability of abradable seal materials for application in centrifugal compressors and steam turbines," in *Proceedings of the Twentieth Turbomachinery Symposium*, pp. 77–90, 1991.

[8] F. Ghasripoor, N. A. Turnquist, M. Kowalczyk, and B. Couture, "Wear Prediction of Strip Seals Through Conductance," in *ASME Turbo Expo 2004: Power for Land, Sea, and Air*, pp. 331–337, June 14–17, 2004.

[9] Z. Mutasim, L. Hsu, and E. Wong, "Evaluation of plasma sprayed abradable coatings," *Surface and Coatings Technology*, 54-55, pp. 39–44, 1992.

[10] U. Rathmann, S. Olmes, and A. Simeon, "Sealing Technology: Rub Test Rig for Abrasive/Abradable Systems," in *ASME Turbo Expo 2007: Power for Land, Sea, and Air*, pp. 223–228, May 14–17, 2007.

[11] D. R. Sporer and L. T. Shiembob, "Alloy Selection for Honeycomb Gas Path Seal Systems," in *ASME Turbo Expo 2004: Power for Land, Sea, and Air*, pp. 763–774, June 14–17, 2004.

[12] T. Pychynski, C. Höfler, and H.-J. Bauer, "Experimental Study on the Friction Contact Between a Labyrinth Seal Fin and a Honeycomb Stator," *Journal of Engineering for Gas Turbines and Power*, vol. 138, no. 6, p. 62501, 2016.

[13] T. Pychynski, *Entwicklung und experimentelle Validierung eines Ansatzes für die Modellierung des Anstreifverhaltens von Labyrinthdichtungen mit Honigwabeneinlaufbelägen*, Band 63, ISBN 978-3-8325-4359-4, Logos Verlag, 2016.

[14] O. Munz, C. Schwitzke, H.-J. Bauer, S. Welzenbach, T. Fischer, and S. Ulan kyzy, "Modelling the Rubbing Process in Labyrinth Seals," in *Proceedings of GPPS Forum 18, Zurich, CH, January 10-12, 2018*, GPPS-2018-0038/ 1-9, 2018.

[15] T. Fischer, S. Welzenbach, F. Meier, E. Werner, S. Ulan kyzy, and O. Munz, "Modeling the rubbing contact in honeycomb seals," *Continuum Mechanics and Thermodynamics*, vol. 30, no. 2, pp. 381–395, 2018.

[16] O. Munz, T. Pychynski, C. Schwitzke, and H.-J. Bauer, "Continued Experimental Study on the Friction Contact between a Labyrinth Seal Fin and a Honeycomb Stator: Slanted Position," *Aerospace*, vol. 5, no. 3, p. 82, 2018.

[17] GasTurb GmbH, "GasTurb 13 Manual: Design and Off-Design Performance of Gas Turbines," *GasTurb GmbH, Aachen, Germany*, 2017.
[18] D. Y. Davis and E. M. Stearns, "Energy Efficient Engine: Flight propulsion system final design and analysis," 1985.
[19] J. W. Chapman and J. S. Litt, "Control Design for an Advanced Geared Turbofan Engine," in *53rd AIAA/SAE/ASEE Joint Propulsion Conference*, c3, American Institute of Aeronautics and Astronautics, Reston, Virginia, 2017.
[20] J. Kurzke and I. Halliwell, *Propulsion and Power*: *An Exploration of Gas Turbine Performance Modeling*, Springer International Publishing, Cham, 2018.
[21] Haynes International, Inc., "HASTELLOY X Alloy," 1997.
[22] Special Metals Corporation, "INCONEL alloy 718," 2007.
[23] L. Hühn, F. Rieger, F. Bleier, C. Schwitzke, H.-J. Bauer, and T. Behnisch, "Extensive Investigations on Radial Crack Formation in Labyrinth Seals of Aircraft Engines," in *Deutscher Luft- und Raumfahrtkongress, Friedrichshafen, Deutschland, 4 - 6 September 2018*, 8 S, Deutsche Gesellschaft für Luft- und Raumfahrt - Lilienthal-Oberth, Bonn, 2018.

APPENDIX

Heat transfer coefficient

$$h_C = h_{C,0}\,\lambda_{eff}\left(\frac{p_c}{E(T_C)}\right)^2 \tag{7}$$

λ_{eff} thermal conductivity,
E Young's modulus of the softer friction partner
$h_{C,0}$ proportionality factor of the heat transfer

Abrasive wear (according to Archard)

$$\dot{w}_a = k_{w,a}\,p_C\,\frac{1}{E}\,v_\varphi \tag{8}$$

$k_{w,a}$ empirical abrasive wear coefficient

Plastic wear

$$\dot{w}_{pl} = \begin{cases} 0, & p_C < k_{w,pl}R_{p02} \\ \left(1 - k_{w,pl}\,\frac{R_{p02}}{p_C}\right)\frac{s}{2\,\pi\,r_{sf}}\,v_\varphi\left(1 - e^{\left(-\frac{\alpha_{ec}\,r_{sf}}{t_{pl}\,v_r}\right)}\right), & p_C \geq k_{w,pl}R_{p02} \end{cases} \tag{9}$$

t_{pl} time constant
$k_{w,pl}$ plastic scaling factor
r_{sf} radius of the seal fin
α_{ec} angle of the contact segment